Simulation of a hydrogen permeation test on a multilayer membrane

J. Bouhattate[1], E. Legrand[1], A. Oudriss[1], S. Frappart[1], J. Creus[1], X. Feaugas[1]
[1] Laboratoire d'Etude des Matériaux en Milieu Agressif, LEMMA, Bat. Marie Curie, Av. Michel Crépeau, 17042 La Rochelle, France

Keywords: Hydrogen Embrittlement, Diffusion, Oxide, Trapping, Modelling

Abstract

To understand a metal susceptibility to Hydrogen Embrittlement (HE), it is important to quantify the diffusion of hydrogen through a metallic membrane. However the parameters directly accessible from electrochemical permeation experiments are the time required for a stream to be observed and the flux saturation corresponding to a steady state. The literature offers different models to obtain the diffusion coefficient from these curves. But this diffusion coefficient is not that of the membrane alone because it also takes into account the surface state and the kinetics of trapping. For some thicknesses of membrane and surface coatings (oxide) this approximation cannot be considered fair. We propose to simulate numerically the influence of the oxide thickness on the effective diffusion coefficient taking into account the trapped hydrogen.

Introduction

Hydrogen is part of many fundamental research investigations in physics and chemistry because of its particular structure. It is also highly inspected in industrial research because of the hydrogen embrittlement that occurs frequently in industrial environments. Studies about hydrogen diffusion in steels are often implemented using permeation tests. It is today employed for many metals (nickel, steels…). Permeation tests allow to easily measure the hydrogen flux through a metallic membrane and can also reveal surface phenomena such as corrosion or impact of an oxide film [2]. The obtained curves provide quantitative information: the steady-state permeation rate, the effective diffusion coefficient D_{eff} and the effective subsurface concentration C_{0eff}. However to access the lattice diffusion coefficient and the average concentration in the membrane, hard hypothesis are generally imposed to interpret experimental data. More specifically, the surface state and the oxide layer haven't been taken into account. Moreover the hydrogen trapped into the microstructure alters the evaluation of the diffusion coefficient.

In order to increase our knowledge of the interactions of hydrogen with steels, the purpose of this research is to simulate the hydrogen diffusion through a metallic membrane with an oxide layer on the exit side by using Comsol Multiphysics. In this work we will explain how the geometry (thickness) affects the experimental data extracted from a hydrogen permeation test.

Permeation Tests

The permeation test is realized through a metallic membrane and is composed of a cell divided in two sections: a charging cell (source of hydrogen) and a detection cell (diffused hydrogen oxidation and creation of a proportional current) divided by a metallic membrane (the sample). Figure 1 represents the principle of hydrogen electrochemical permeation test. The electrochemical reaction characteristics are the electrochemical adsorption and the reduction of the proton in the charging cell in acid media:

$$2H^+ + 2e^- \rightarrow H_2 \quad (1)$$

A part of the hydrogen is then absorbed and diffused through the steel membrane. On the detection side, the anodic polarisation oxidizes the diffused hydrogen generating an anodic current:

$$H_{ads} \rightarrow H^+ + e^- \quad (2)$$

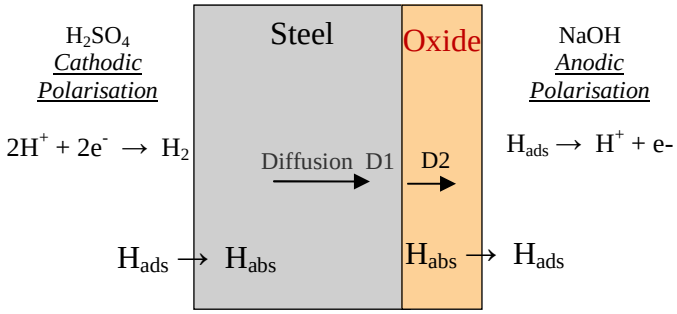

Figure 1: Principle of hydrogen electrochemical permeation test

The charging solution is acidique, such as sulfuric acid H_2SO_4 0.5M [3-5]. The usual detection solution is NaOH 0.1M [1,4,6,11,12].

The presence of a passive layer could decrease the hydrogen oxidation rate due to hydrogen recombination which leads to an erroneous evolution of solubility and diffusion rate. Some authors [6,13] have used an electrolytic palladium layer to ensure the oxidization of all the hydrogen and to avoid the molecular recombination and the creation of an oxide layer. But this technique is subjective because it modifies the boundary conditions at the interface, and even if diffusion properties through palladium are well known [1], these electrolytic coatings bring supplementary defects that could interact with diffused hydrogen species.

Diffusion Laws

In the classical permeation technique by Devanathan and Stachursky [1,14], a thin metal membrane of thickness *e* is placed between two independent electrochemical cells. Hydrogen is introduced on the entry side *(x=0)*, diffuses through the membrane and is immediately oxidized on the exit side (*x=e*).

The convenience of permeation techniques used in this work, is based on the presumption that the conditions of diffusion are established beneath the entry side, where the concentration of hydrogen C_0 is supposed to be constant.

The main problem consists in the presence of a passive layer on the exit side. The stability of the oxide layer may control the diffusion phenomenon and can have consequences on the experimental results. Specially the diffusion curves correspond to a multilayered system with two different materials and their own diffusion coefficient: D_L for the steel and D_{ox} for the oxide layer.

Thus, only an effective diffusion coefficient D_{eff} can be determined, if we consider the system (steel + oxide layer) as a homogeneous representative volume element (HRVE). However, in our computational model we have to discern the apparent diffusion coefficient D_{app} which is related to the node calculations.

Fick's laws (3) (4) describe diffusion into the multilayered system assuming that there is no hydrogen trapping and the diffusion is unidirectional:

$$J(x,t) = -D_{app}\frac{\partial C(x,t)}{\partial x} \quad (3)$$

$$\frac{\partial C}{\partial t} = D_{app}\frac{\partial^2 C}{\partial x^2} \quad (4)$$

Trapping Model

The trapping model used in this work is based on the one presented by Oriani [16] and developed by Krom [16]. This model defines two types of traps in steels: reversible and unreversible traps. While in reversible traps, hydrogen atoms have a weaker link and therefore can be easily released and replaced and may be achieving a steady state. However, hydrogen atoms trapped in unreversible sites are less likely to be released. Unreversible traps are for example dislocations or grain boundaries.

For coherent purposes, all variables linked to lattice sites will have the subscript ‘L’, while variables linked to trapping sites will have the subscript ‘T’.

Fick’s laws then become:

$$\vec{j} = -D_L \times \overrightarrow{grad}(C_L) \quad (5)$$

$$\frac{\partial C}{\partial t} = div(-D_L \times \overrightarrow{grad}(C_L)) \quad (6)$$

When hydrogen is trapped, we have to consider the hydrogen concentration as the sum of two concentrations: the lattice and the trapped concentrations of hydrogen.
We then have:

$$C = C_T + C_L \quad (7)$$

Equation (6) can be derived and we finally get:

$$\frac{\partial C_L}{\partial t} - D_{app}\Delta C_L = 0 \quad (8)$$

With D_{app} the apparent diffusion coefficient:

$$D_{app} = \frac{D_L}{1 + \frac{\partial C_T}{\partial C_L}} \quad (9)$$

Lattice and trapping sites present different energy states. Lattice sites have a lower energy than trapping sites. ΔE_T is called the trap binding energy and corresponds to the difference between the activation energy to move from a trap site and the activation energy to move from a lattice site [17]. In our work ΔE_T=-0.3eV.

The number of hydrogen atoms moving from L sites to T sites is proportional to the lattice hydrogen concentration C_L.

The occupancy of lattice sites is often $\theta_L << 1$. The number of traps N_T is very small compared to the number of lattice sites N_L. Moreover, if we consider $\theta_T << 1$, and in case of stationary state, $\frac{\partial C_T}{\partial t} = 0$, we get:

$$C_T = \frac{N_T}{1 + \frac{N_L}{K_T C_L}} \quad \text{with} \quad K_T = \exp\left(-\frac{\Delta E_T}{k_B T}\right) \quad (10)$$

The ratio $\frac{\partial C_T}{\partial C_L}$, which depends on C_T and C_L can now be calculated and fnally, we have:

$$D_{app} = \frac{D_L}{1 + \frac{C_T\left(1 - \frac{C_T}{N_T}\right)}{C_L}} \quad (11)$$

Numerical Model

An FEM model was proposed using Comsol Multiphysics software to determine the repercussion of the coating layer on the hydrogen diffusion and on the effective diffusion coefficient D_{eff}. The studied model is described in figure 2. We used a quadratic meshing in a transient analysis of the diffusion module with a linear system solver.

The boundary conditions are C_0=5mol/m^3, C_S=0mol/m^3. We considered martensitic steels with a diffusion coefficient of D_L=1.45×10^{-9}m^2/s [17]. We modified the oxide layer property D_{ox} so that $D_{ox} \in [1\times10^{-10}; 1\times10^{-16}]$ m^2/s [18]. Doing so enabled us to determine the effects of the oxide layer on the effective diffusion coefficient D_{eff}. The steel thickness is 1mm and the oxide layer thicknesses range from 5nm to 100nm. Table 1 recapitulates all the constants [17].

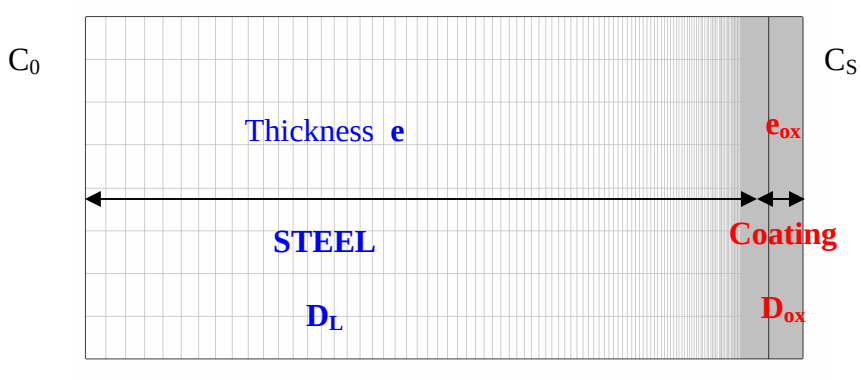

Figure 2: Geometrical data of the problem and 2D meshing

Table1: List of constants used in the numerical model

D_L	1.45×10^{-9} m^2/s
N_T	21 mol/m^3
N_L	2.108×10^{5} mol/m^3
ΔE_T	-0.32 eV
K_b	1.3806×10^{-23} J/K
T	300 K
C_0	1 mol/m^3
C_S	0 mol/m^3

Results and Discussion

The evolution of the flux at the exit side as a function of thicknesses for two types of oxide layers ($D_{ox}=10^{-12}m^2/s$ and $D_{ox}=10^{-14}m^2/s$) is plotted in figure 3. We can easily notice the decrease of the flux as e_{ox} increases when the oxide diffusion coefficient is largely inferior to the membrane diffusion coefficient. Also from figure 4, which represents the evolution of flux at the exit side in function of D_{ox} for two thicknesses (e_{ox}=5nm and e_{ox}=50nm), it is clear that the oxide diffusion coefficient affects tremendously the flux evolution for thicker oxide layers.

If we set $R=D_L/D_{ox}$, it seems that for R<1000, the oxide diffusion coefficient does not influence the flux evolution for any thicknesses of the oxide layer.

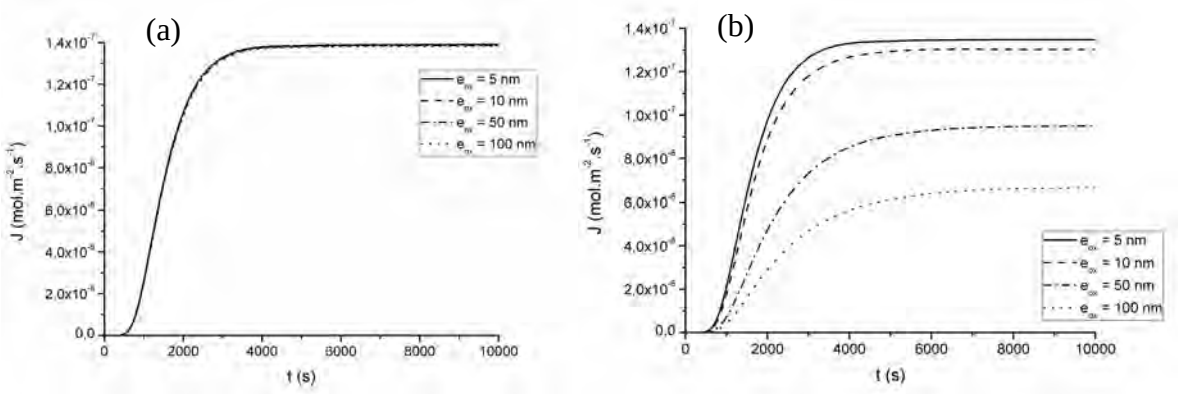

Figure 3: Evolution of the flux at the exit side as a function time for several thicknesses for two types of oxide layers (a) $D_{ox}=10^{-12}m^2/s$ and (b) $D_{ox}=10^{-14}m^2/s$

For D_{ox} ϵ $[10^{-10}; 10^{-16}]$ m^2/s, the steady state flux decreases by 86% and 99% for an oxide layer thickness of respectively 5 nm and 50 nm.

In experimental approaches [17], the evolution of flux enables the calculation of the effective diffusion coefficient. Several methods exist to calculate D_{eff} from experimental results from a specific time taken on the graph of the diffusive flux with respect to time.

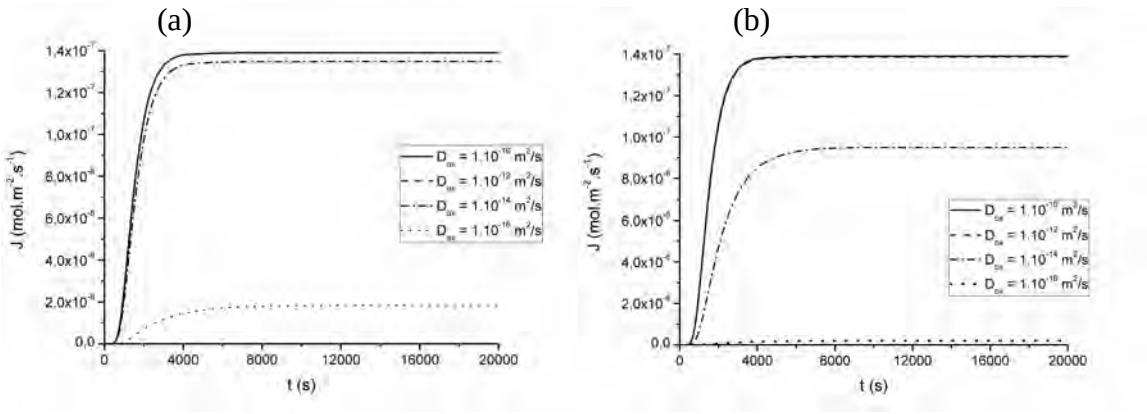

Figure 4: Evolution of the flux at the exit side as a function of time for several D_{ox} for two thicknesses of oxide layers (a) e_{ox}=5nm and (b) e_{ox}=50nm

In our work, we used the "breakthrough-time" method; D_{eff} is calculated with the time required to reach 10% of the maximum flux, given by the stationary part of the curve.
Knowing t_b, the effective diffusion coefficient is given by:

$$D_{eff} = \frac{L^2}{15.3 \times t_b} \quad (12)$$

Here, L is the total width of our system.

Figure 5 depicts the variation of D_{eff} in function of the oxide diffusion coefficient for several thicknesses. It appears that D_{eff} is about twenty times smaller than D_L due to trapping. However, all the curves have the same aspect, for all thicknesses. It seems that the oxide layer drops the effective diffusion coefficient. The main difference resides in the fact that for thicker coatings, D_{eff} will drop for higher D_{ox}. But all the curves meet at a D_{eff} of $5.5\times10^{-11}m^2/s$. The loss in D_{eff} induced by the trapping phenomenon is about twenty times greater that the effect due to the oxide layer for any thickness of the oxide and for our conditions.

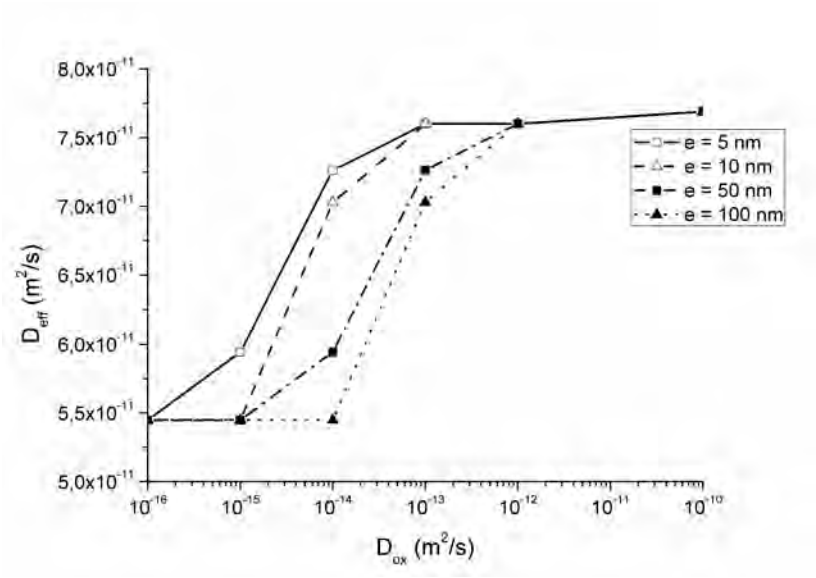

Figure 5: D_{eff} in function of D_{ox} for several oxide thicknesses

Experimentally, the initial concentration of hydrogen cannot be exactly known. However, it is possible to calculate it using D_{eff}. Since this concentration isn't the exact initial value, in this work, it will be called the effective initial concentration C_{0eff}, which is calculated as follow:

$$C_{0eff} = \frac{L \times J_{\infty}}{D_{eff}} \quad (13)$$

This calculation enables us to grasp the effect of trapping in figure 6. This figure represents the evolution of C_{0eff} in function of D_{ox} for several thicknesses. The imposed concentration at the entrance of our model is C_0 = 1mol/m^3 whereas C_{0eff} reaches 1.8mol/m^3 for D_{ox} close to D_L (10^{-10}m^2/s) due to trapped hydrogen. Once more the thickness of the oxide layer affects the drop of the C_{0eff}. However, when the oxide layer diffusion coefficient is below $D_{ox} = 10^{-14}$m^2/s, the calculated concentration C_{0eff} becomes inferior to the real entrance concentration C_0. Then the presence of the oxide has the inverse effect of the trapping on C_{0eff}. For real coating (thickness<10nm [19]), it is clear that above $D_{ox}>10^{-14}$m^2/s, the trapping will have a greater effect whereas for $D_{ox}<10^{-14}$m^2/s, the modification of C_{0eff} is imputed to the oxide layer.

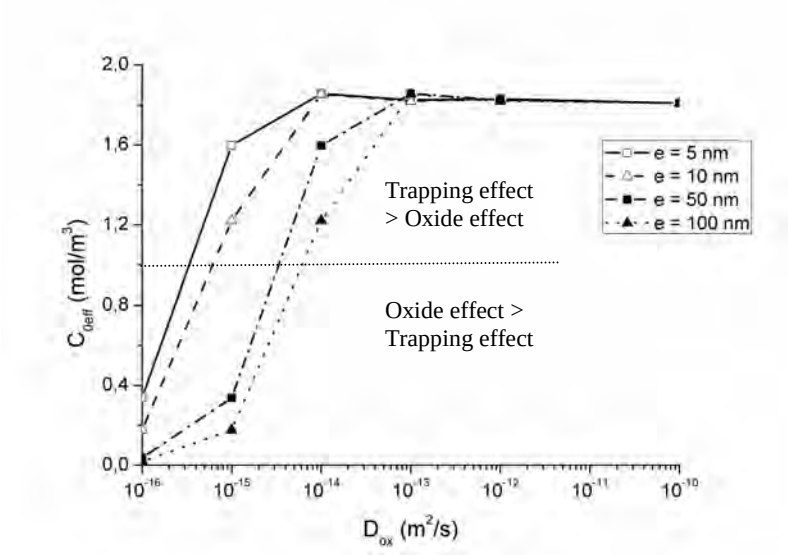

Figure 6: C_{0eff} in function of D_{ox} for several oxide thicknesses

Conclusion

The conducted work in the paper was performed to study the information collected during experimental permeation tests. Knowing that the obtained curves during permeation tests provide us with quantitative information: the effective diffusion coefficient, the subsurface concentration C_0 and the steady-state permeation rate; it is interesting to take into account the effects of the surface state and more specifically thickness and the type of the oxide layer. We were able to determine that the thickness and the diffusion coefficient of the oxide layers affect the evolution of the flux when D_{ox} is a thousand time smaller than D_L, which occurs most of the time in reality. From the flux curves we computed the effective diffusion coefficient D_{eff} and the calculated initial concentration C_{0eff}, which were also altered by the geometry of the oxide coating and by the trapped hydrogen. The trapping model was based on Oriani's model and enabled us to estimate the evolution of the average concentrations of trapped and lattice of hydrogen.

References

[1] M.A.V. Devanathan, Z. Stachursky, The adsorption and diffusion of electrolytic hydrogen in palladium, *The Royal Society*, Vol.270, pp 90-102 (1962)

[2] T. Casanova, J. Crousier, The influence of an oxide layer on the hydrogen permeation through steel, *Corros. Sci.*, Vol.38, N°9, pp 1535-1544 (1996)

[3] J. Yao, J.R. Cahoon, Experimental studies of grain boundary diffusion of hydrogen in metals, *Acta Met. And Mat.*, Vol. 39, No 1, pp 119-126 (1991)

[4] N. Parvathavarthini, S. Saroja, R.K. Dayal, Influence of microstructure on hydrogen permeability of 9%Cr-1%Mo ferritic steel, *J. Nucl. Mat.*, Vol. 264, pp 35-47 (1999)

[5] A.M. Brass, J. Chene, Influence of hydrogen transport and trapping in ferritic steels with electrochemical permeation technic, *Env. Induced Crac. Of Mat.*, pp215-225 (2008)

[6] M. Jerome, Interactions Hydrogène-Métal et permeation électrochimique, *Mémoire d'HDR*, Université de technologie de Compiègne (2003)

[7] C. Ly, Caractérisation d'aciers à très haute limite d'élasticité vis-à-vis de la fragilisation par l'hydrogène, *Thèse de Doctorat*, Ecole Centrale Paris (2009)

[8] M. Garet, A.M. Brass, C. Haut, F. Guttierez-Solana, Hydrogen trapping on non metallic inclusions in Cr-Mo low alloy steels, *Corros. Sci.*, Vol.40, N°7, pp 1073-1086 (1998)

[9] Y.F. Cheng, Analysis of electrochemical hydrogen permeation through X-65 pipeline steel and its implications on pipeline stress corrosion cracking, *Int. J. of Hydrogen Energy*, Vol.32, pp 1269-1276 (2006)

[10] V.P. Ramunni, T. De Paiva Coelho, P.E.V. de Miranda, Interaction of hydrogen with the microstructure of low-carbon steel, *Mater. Sci. Eng. A*, 435-436, pp 504-514 (2006)

[11] K. Banerjee, U.K. Chetterjee, Hydrogen permeation and hydrogen content under cathodic charging in HSLA 80 and HSLA 100 steels, *Scripta Mater.*, Vol.44, pp 213-216, (2001)

[12] L.W. Tsay, W.C. Lee, W.C. Luu, J.K. Wu, Effect of hydrogen environment on the notched tensile properties of T-250 maraging steel annealed by laser treatment, *Corro. Sci.*, Vol.44, pp 1311-1327 (2002)

[13] P. Manolatos, M. Jerome, J. Galland, Necessity of a palladium coating to ensure hydrogen oxidation during electrochemical permeation measurements on iron, *Electrochem. Acta*, Vol.40, N°7, pp 867-871 (1995)

[14] M.A.V Devanathan, Z. Stachursky, The mechanism of hydrogen evolution on iron in acid solutions by determination of permeation rates, *J. electrochem. Soc.*, Vol.111, N°5, pp 619-623 (1964)

[15] R.A. Oriani. The Diffusion and Trapping of Hydrogen in Steel, *Acta Metallurgica*, 18 (1), January 1970, pp. 147-157

[16] A.H.M. Krom, A.D. Bakker. Hydrogen trapping Models in Steel, *Metal. and Mat. Trans. B: Process Metallurgy and Materials Processing Science*, 31 (6), December 2000, pp. 1475-1482

[17] S. Frappart, X. Feaugas, J. Creus, F. Thebault, L. Delattre, H. Marchebois, Study of the hydrogen diffusion and segregation into Fe-C-Mo martensitic HSLA steel using electrochemical permeation test, *J. Phys. Chem. Solids* (2010) submitted

[18] V. Olden, C. Thaullow, R. Johensen, Modelling of hydrogen diffusion and hydrogen induced cracking in supermartensitic and duplex stainless steels, *Materials and Design*, 29 (2008) pp. 1934-1948

[19] P. Bruzzoni, R. Garavaglia, Anodic iron oxide films and their effect on the hydrogen permeation through steel, *Corros. Sci.*, Vol. 33, No.11 (1992) pp. 1797 – 1807